

Article

Photocatalytic Inactivation of Bacteriophage f2 with $\text{Ag}_3\text{PO}_4/\text{g-C}_3\text{N}_4$ Composite under Visible Light Irradiation: Performance and Mechanism

Rong Cheng ^{*}, Liang-jie Shen, Jin-hui Yu, Shao-yu Xiang and Xiang Zheng ^{*}

School of Environment and Natural Resources, Renmin University of China, Beijing 100872, China; shenliangjie@ruc.edu.cn (L.-j.S.); yjhlyily@163.com (J.-h.Y.); xiangshaoyu@ruc.edu.cn (S.-y.X.)

^{*} Correspondence: chengrong@ruc.edu.cn (R.C.); zhengxiang@ruc.edu.cn (X.Z.);

Tel.: +86-185-1162-4185 (R.C.); +86-189-1190-2287 (X.Z.)

Received: 27 August 2018; Accepted: 18 September 2018; Published: 20 September 2018



Abstract: Water-borne virus pollution has caused great harm and attracted widespread attention in many countries. Visible-light-driven photocatalysis is considered as a promising process for disinfection. In this study, $\text{Ag}_3\text{PO}_4/\text{g-C}_3\text{N}_4$ (AgCN) composites were synthesized by hydrothermal method. The photocatalytic disinfection was investigated using bacteriophage f2 as the model virus. Moreover, the effects of pH and humic acid on photocatalytic disinfection were studied. Meanwhile, the mechanism of enhanced disinfection by $\text{Ag}_3\text{PO}_4/\text{g-C}_3\text{N}_4$ was systematically investigated by radical scavenger experiments. The results show that Ag_3PO_4 particles were uniformly distributed on $\text{g-C}_3\text{N}_4$ sheets. By means of photoluminescence spectrometer analysis, it is confirmed that a lower carrier recombination rate for $\text{Ag}_3\text{PO}_4/\text{g-C}_3\text{N}_4$ was achieved compared with Ag_3PO_3 and $\text{g-C}_3\text{N}_4$. Meanwhile, complete inactivation of f2 with concentration of 3×10^6 PFU/mL was reached within 80 min in the presence of $\text{Ag}_3\text{PO}_4/\text{g-C}_3\text{N}_4$ composite. The pH had little effect on removal efficiency overall, while the existence of humic acid resulted in a significant negative effect on the inactivation of f2 due to the optical shielding and absorption of humic acid. Recycling tests of $\text{Ag}_3\text{PO}_4/\text{g-C}_3\text{N}_4$ confirmed that $\text{Ag}_3\text{PO}_4/\text{g-C}_3\text{N}_4$ presented superior stability. The results from radical scavenger experiments indicated that holes (h^+) and hydroxyl radicals ($\cdot\text{OH}$) played important roles in photocatalytic disinfection process.

Keywords: photocatalysis; Ag_3PO_4 ; $\text{g-C}_3\text{N}_4$; bacteriophage f2; mechanism

1. Introduction

Water is the source of life. Due to the invalid treatment of sewage, reclaimed water, and even drinking water, pathogenic microorganism pollution problems of water bodies occur frequently. Water microbial pollution could directly affect ecosystem stability and health of residents [1]. Therefore, to ensuring the microbiological safety of water bodies is a top priority for any country or region. Pathogenic microorganisms in water, even drinking water, including bacteria, pathogenic protozoa (*Cryptosporidium*, *Giardia*, etc.), viruses, etc., have received much attention. Especially for waterborne viruses, their illness risk is assessed to be $10\text{--}10^4$ times higher at a similar level of exposure compared with bacteria, and has aroused strong concern in countries around the world [2]. Therefore, efficient removal of viruses from water is of great significance, especially in developing countries and rural areas.

Over the past decades, traditional disinfection methods can inactivate viruses to some extent. Chlorination, chlorine dioxide [3], ozone, bromide, and iodide [4], as well as combined technologies [5], are widely used to control waterborne pathogens, even though many byproducts with harmful long-term effects are produced, along with operational problems of onsite generation [6].

Therefore, there is an extreme demand for a low-budget, efficient and environmentally-friendly viral inactivation technology.

Photocatalysis is a promising technology, which can produce a kind of active free radicals under the irradiation of a certain wavelength of light for the degradation of organic matter and microorganism inactivation and other fields under a mild condition [7]. In the whole photocatalytic process, the excellent photocatalyst is one of the key factors to improve the system performance and reduce energy consumption. Therefore, many scholars are exploring new and efficient photocatalysts to further narrow the distance of practical applications of photocatalytic technology. Fortunately, in recent years, graphite-like nitrogen carbide ($g\text{-C}_3\text{N}_4$), a kind of nonmetallic photocatalyst, has attracted great attention because of its appropriate band gap (2.7 eV), low cost, non-toxicity, and good photochemical and chemical stability [8–11]. However, there are still defects in all photocatalytic materials, such as high recombination rate of photogenerated electrons and holes, and insufficient visible-light absorption (<470 nm). In view of the above problems, several strategies have been used, such as vacancy defects [12,13], element doping [14,15], and semiconductor recombination [16,17]. In particular, semiconductor recombination has been widely studied in virtue of its simple preparation and obvious widening of light response range.

As a kind of new visible-light-driven photosensitizers, Ag_3PO_4 -based photocatalysts have attracted attention due to their faultless photocatalytic oxidation activity for degradation of organic pollutants [18] and antibacterial activities [19]. Moreover, strong visible light absorption response and photochemical stability characterize Ag_3PO_4 photocatalysts. However, for most photocatalysts, there is also the congenital deficiency of high electron–hole recombination rate and difficult recycling process.

Bearing the above in mind, the central purpose of this study was to synthesize $\text{Ag}_3\text{PO}_4/g\text{-C}_3\text{N}_4$ composite photocatalysts, which were used for the photocatalytic disinfection of bacteriophage f2, a widely used model virus that has similar physiological and biochemical characteristics to enterovirus. Moreover, the mechanism of photocatalytic disinfection was investigated thoroughly.

2. Results and Discussion

2.1. Characterization of As-Prepared Photocatalysts

2.1.1. X-ray Diffraction (XRD) Analysis

The phase structures of the as-prepared $g\text{-C}_3\text{N}_4$, Ag_3PO_4 , and AgCN composite were analyzed by XRD instrument and the results are shown in Figure 1.

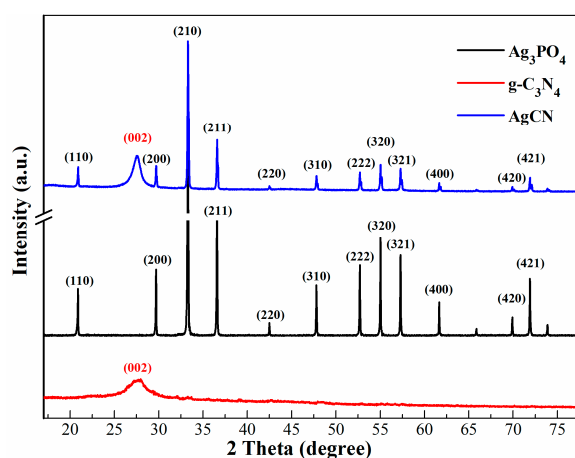


Figure 1. XRD patterns of the synthesized Ag_3PO_4 (black line) and $g\text{-C}_3\text{N}_4$ (red line) and AgCN (blue line) composite.

The peaks at 2θ of 20.87° , 29.68° , 33.30° , 36.66° , 42.48° , 47.91° , 52.83° , 55.08° , 57.42° , 61.66° , 69.9° , and 72.02° could be assigned to (110), (200), (210), (211), (220), (310), (222), (320), (321), (400), (420), and (421) crystal planes of the Ag_3PO_4 particles, respectively, which is consistent with the value reported by Joint Committee on Powder Diffraction Standards (JCPDS) (No. 74–1876, $a = b = c = 5.995$ nm) [20]. As for $g\text{-C}_3\text{N}_4$, the strong diffraction angle at 27.3° , corresponding to 0.325 nm, was indexed as (002) diffraction plane (JCPDS 87–1526) [21,22]. Furthermore, all diffraction peaks of prepared AgCN composite are highly consistent with that of $g\text{-C}_3\text{N}_4$ and body-centered cubic Ag_3PO_4 , which confirmed that the combination did not destroy the structure of $g\text{-C}_3\text{N}_4$. No impurity phase was found in the AgCN composites.

2.1.2. Morphology Analysis

Figure 2 depicts the typical scanning electron microscope (SEM) images of the Ag_3PO_4 , $g\text{-C}_3\text{N}_4$, and AgCN composite. The SEM images (Figure 2a,b) indicate that Ag_3PO_4 particles present a uniform spherical particle with a diameter of about 200 nm, and $g\text{-C}_3\text{N}_4$ displays a lamellar structure with many pores, which is beneficial to the uniform loading of Ag_3PO_4 particles. As indicated in Figure 2c, Ag_3PO_4 particles dispersed on the outer surface of $g\text{-C}_3\text{N}_4$ nanosheets. Figure 2d–g shows the elemental mappings of AgCN photocatalysts, indicating the homogeneous distribution of C, N, Ag, and P elements. Figure 2c (inset Energy Dispersive Spectrometer (EDS) spectra) shows the EDS spectra of AgCN composites, which indicates that the samples were very pure without any other elements. Meanwhile, from the element content table, the mass ratio of carbon to silver could be calculated as about $33.86 \pm 3\%$, which is relatively close to the theoretical value.

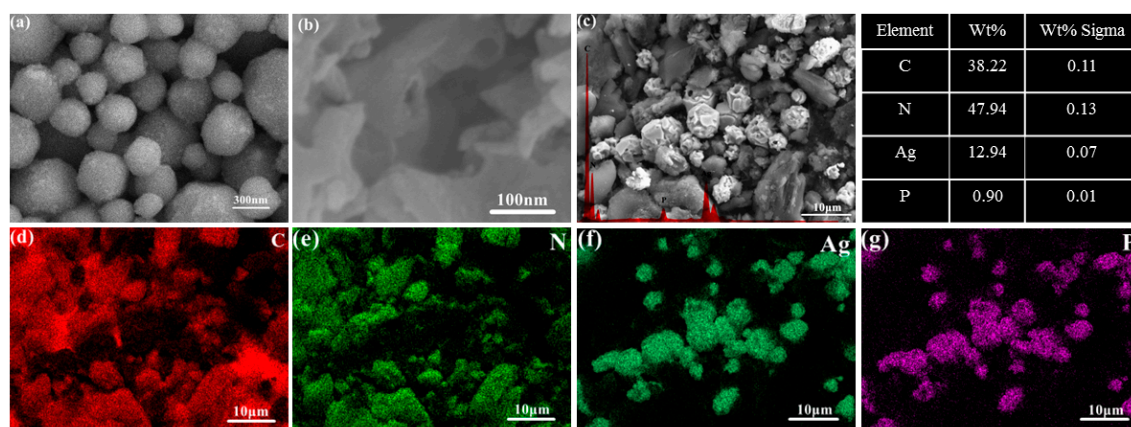


Figure 2. SEM images of: Ag_3PO_4 (a); $g\text{-C}_3\text{N}_4$ (b); and AgCN (inset with element ratio) (c); and corresponding element mapping of AgCN composite (d–g).

2.1.3. Pore Structure Analysis

The textural property of as-prepared $g\text{-C}_3\text{N}_4$ and AgCN composite was characterized by the nitrogen gas porosimetry measurement. The obtained sorption isotherms, Barrett-Joyner-Halenda (BJH) pore-size distribution curves, and value of Brunauer-Emmett-Teller (BET) test are shown in Figure 3a–c. Obviously, both prepared materials exhibit type IV isotherms with H3 hysteresis loops, indicating their main multi-micropore structure (Figure 3a). Two kinds of mesopores focused on 3.5 and 18.0 nm are detected in Figure 3b, inspired by the soft templates of the produced ammonia and carbon dioxide during the process of urea polymerization from low temperature to high temperature [23]. This excellent porosity property makes the prepared $g\text{-C}_3\text{N}_4$ achieve much larger BET surface area ($78.2 \text{ m}^2 \cdot \text{g}^{-1}$) and higher pore volume ($0.336 \text{ cm}^3 \cdot \text{g}^{-1}$). Naturally, the Ag_3PO_4 particles were in situ formed on the surface and internal structure of $g\text{-C}_3\text{N}_4$ sheets, and the prepared AgCN photocatalyst also shows two types of porous structure, but the pore diameter (2.194 nm) and pore volume ($0.193 \text{ cm}^3 \cdot \text{g}^{-1}$) are lower than those of the $g\text{-C}_3\text{N}_4$ photocatalyst (Figure 3c).

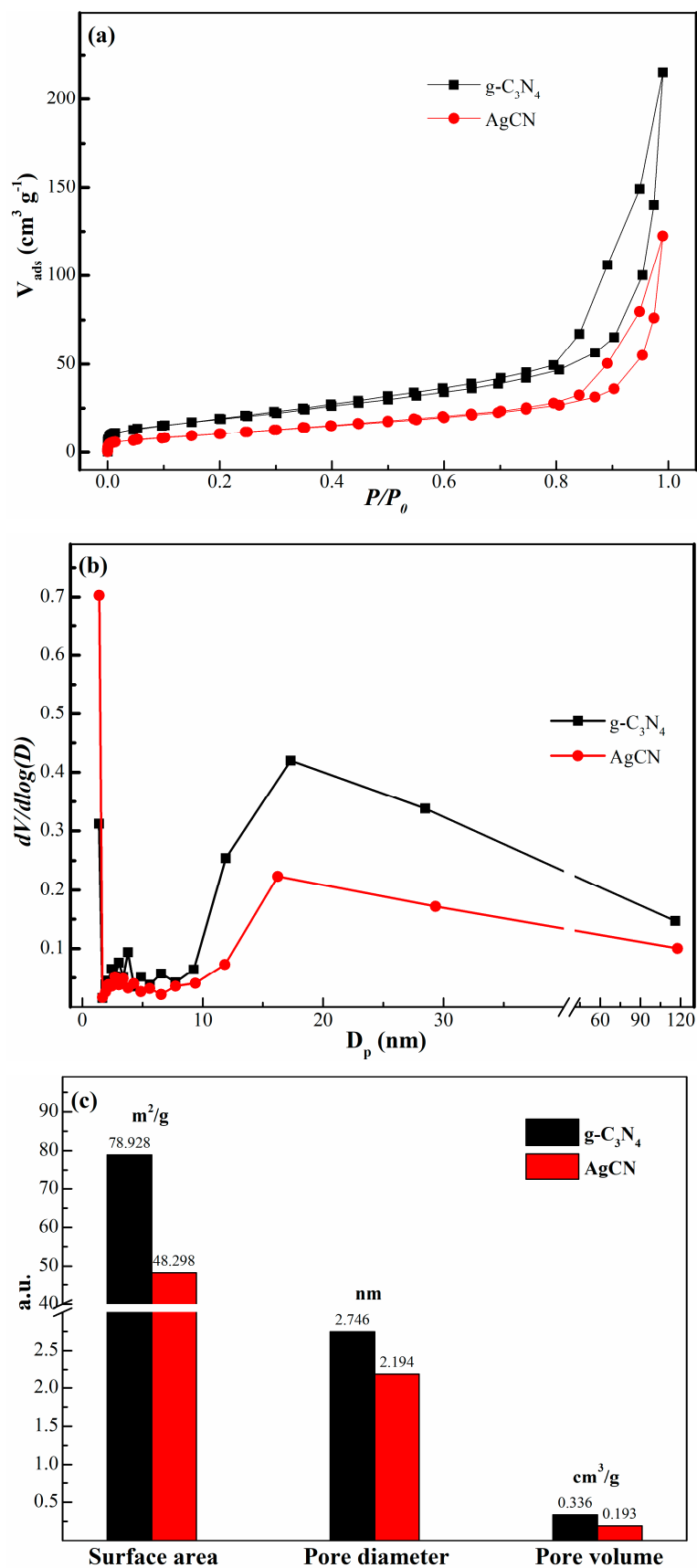


Figure 3. Nitrogen gas adsorption–desorption isotherms (a); BJH pore-size distribution curves (b); and (c) S_{BET} of the $g-C_3N_4$ and AgCN composite photocatalysts.

2.1.4. DRS Analysis

To understand the optical response characteristics of the photocatalysts, Ultraviolet-visible (UV-vis) diffuse reflectance spectra measurement (DRS) was applied to study the light absorption property of the g-C₃N₄, Ag₃PO₄ and AgCN composite. In Figure 4a, pristine g-C₃N₄ reveals a distinct absorption band at ~475 nm, which is consistent with previous work [24]. In contrast to g-C₃N₄ photocatalysts, the Ag₃PO₄ particles are significantly proven to have a strong visible light response behavior and subsequently show strong absorption edge at 546 nm in the visible light band. When the AgCN composite is formed, the materials appear to be able to respond to light, indicating wider response of the absorption edges and enhanced light absorption in the visible range compared to g-C₃N₄ [16,20,25]. The absorption spectrum of AgCN composites also has a strong photo-absorption edge around 500 nm in the visible-light region, which can be ascribed to the combination of Ag₃PO₄ particles [20]. The AgCN composite exhibits a higher visible-light driven photocatalytic potential, which presents the synergistic features of g-C₃N₄ and Ag₃PO₄ photocatalysts.

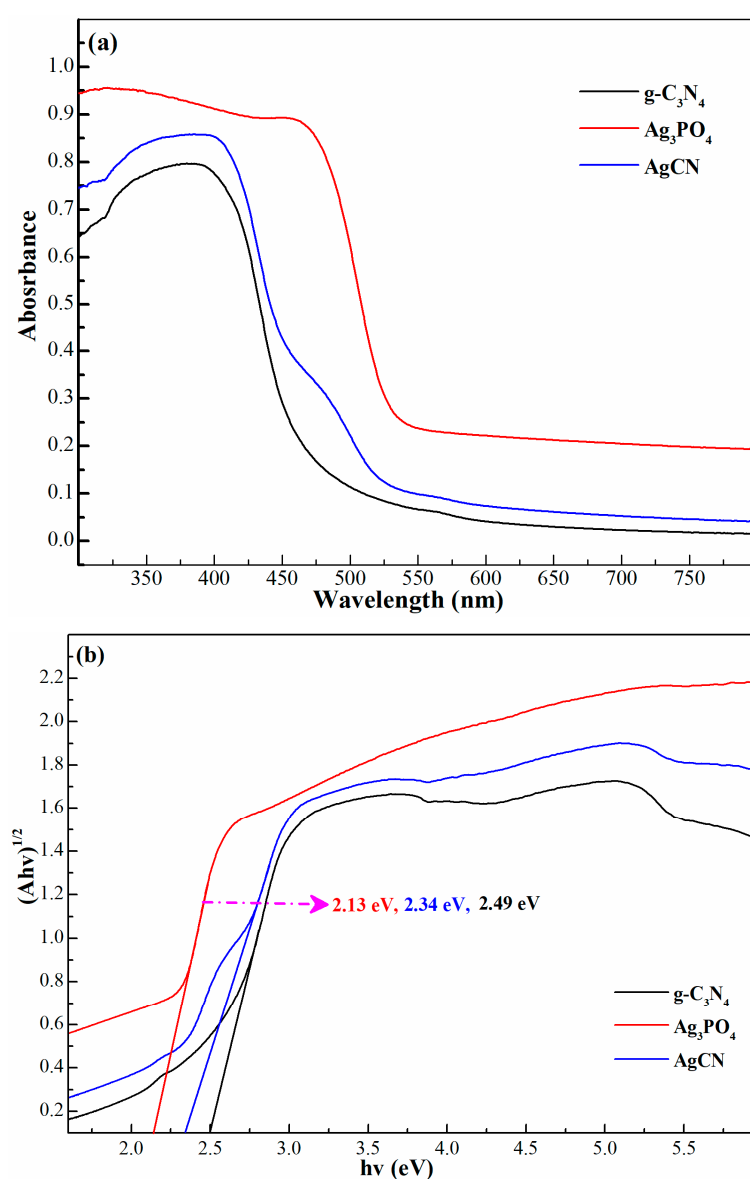


Figure 4. UV-vis diffuse reflectance spectra patterns (a); and band gap energies (b) of the g-C₃N₄ (black line), Ag₃PO₄ (red line) and AgCN photocatalysts (blue line).

Meanwhile, to visually understand the optical properties of the different materials, the Oregan and Gratzel method was used to calculate their bandgaps, as shown in Equation (1) [26]:

$$(\alpha hv)^{n/2} = A(hv - E_g) \quad (1)$$

where α is the absorption coefficient, hv is the light frequency, E_g is the band gap energy, and n is equal to 1 or 4, depending on whether the transition is direct or indirect, respectively. The type of electron transition in g-C₃N₄ and Ag₃PO₄ are both direct transition between bands. According to Equation (1), E_g of the g-C₃N₄ and Ag₃PO₄ photocatalysts can be calculated by a plot of $(Ahv)^{1/2}$ versus photon energy (hv), as shown in Figure 4b. The E_g value of g-C₃N₄, Ag₃PO₄, and AgCN photocatalysts are 2.49, 2.13, and 2.34 eV, respectively.

2.1.5. PLS Analysis

Photoluminescence spectral (PLS) analysis was carried out to reveal the migration, transfer, and recombination processes of photoinduced electron–hole pairs in the composite system. Figure 5 depicts the PLS spectra of g-C₃N₄ and AgCN photocatalysts with an excitation wavelength of 325 nm at room temperature. In Figure 5, AgCN composite has a similar fluorescence emission characteristic to that of g-C₃N₄. However, the PLS emission intensity of AgCN composite photocatalyst decreased by ca. 48% compared to that of the g-C₃N₄ photocatalyst, which means that AgCN composite has a much lower recombination rate of photoinduced electron–hole pairs and further presents a higher photocatalytic oxidation ability.

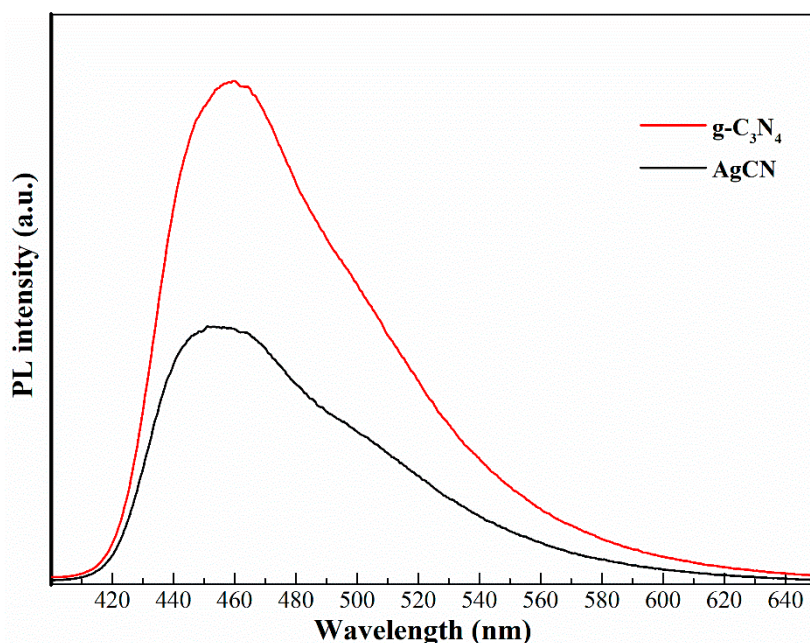


Figure 5. Photoluminescence spectrum of g-C₃N₄ and AgCN photocatalysts.

2.2. Photocatalytic Disinfection Performance to Bacteriophage f2

2.2.1. Kinetics Analysis of Photocatalytic Inactivation Process

The inactivation activities towards representative bacteriophage f2 were investigated under visible light irradiation. Meanwhile, the inactivation efficiency in the dark and under visible light of the three catalysts (g-C₃N₄, Ag₃PO₄, and AgCN) were compared, as shown in Figure 6.

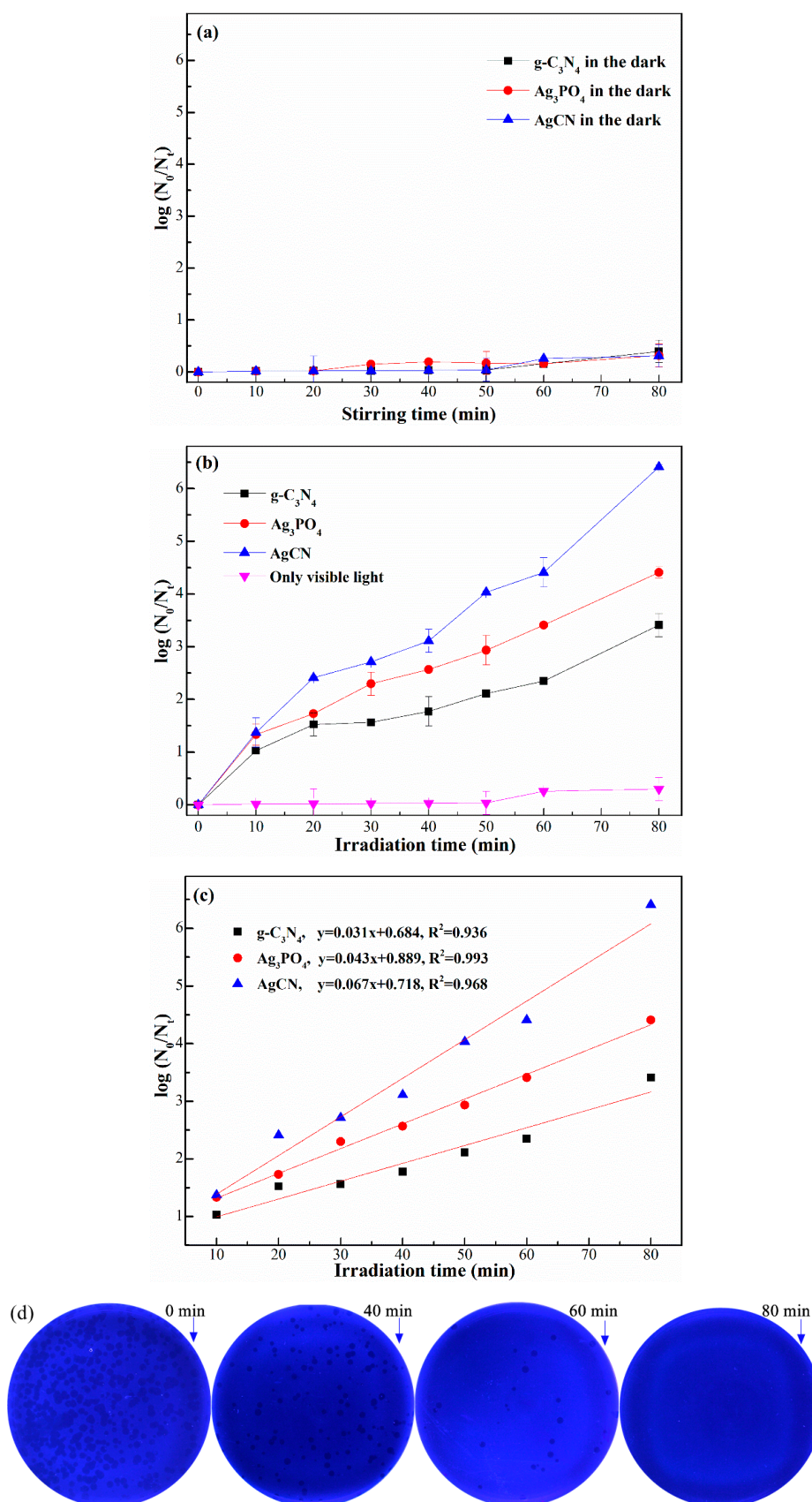


Figure 6. Inactivation efficiency toward bacteriophage f2 by different materials in the dark (a); under visible light irradiation (b); linear fitting of the kinetic curves of inactivation (c); and images of counting plate at different times (d).

In Figure 6a, we can clearly see that the inactivation effects are negligible (<0.5 log) for all photocatalysts in the dark, which indicates that the materials themselves have no effect on the virus. Meanwhile, the removal of bacteriophage f2 under only visible light is also negligible, as shown in Figure 6b. On the contrary, the photocatalytic inactivation efficiency by g-C₃N₄, Ag₃PO₄, and AgCN photocatalysts reaches 3.6 log, 4.5 log, and 6.5 log within 80 min, respectively, under the visible light irradiation. It is clear that AgCN composite photocatalysts present higher photocatalytic activity than the other two photocatalysts. Meanwhile, the shorter inactivation irradiation time of AgCN composite was achieved compared with other photocatalysts, which indicates the lower energy consumption for the AgCN composite photocatalysts [25,27]. It is worth mentioning that the blind pursuit of narrow band gap (E_g) is not desirable to some extent. Combined with the content in Figure 4, it is obvious that the excellent photocatalytic oxidation effect is not directly proportional to the band gap, but is also related to other factors such as position of conduction/valence band, and carrier recombination rate. In addition, to directly reflect the removal rate of different photocatalysts, the Chick–Watson model ($\log(N_0/N) = kt + c$), one of the most fundamental and simplest models to analyze the principle of disinfection kinetics, was used to explain the removal effect, as shown in Figure 6c. It is obvious that the experimental results are consistent with the Chick–Watson model ($R^2 > 0.935$). Moreover, the rate constant (k) of AgCN composite photocatalysts (0.067 min^{-1}) is about 1.5 times that of single photocatalysts. In Figure 6d, we can see that, with the general increase of irradiation time, the amount of the virus cultured obviously decreased, which visibly indicated the excellent inactivation performance of the AgCN composite.

2.2.2. Effect of pH Value

The disinfection efficiencies of as-prepared photocatalysts under a wide pH range from 5.0 to 9.0 were explored and the obtained results are displayed in Figure 7. In Figure 7, it is obvious that the removal efficiency of bacteriophage f2 reached 6.5 log within 80 min under the irradiation of visible light. The effect of pH on the efficiency of photocatalytic disinfection is not significant in the selected range from 5.0 to 9.0. Meanwhile, it is worth pointing out that, in the initial 40 min, the inactivation efficiency in acidic condition is higher than that in neutral or alkaline conditions, which may be due to the more hydroxyl radicals ($\cdot\text{OH}$) generated under acidic condition. The strong oxidizing property of hydroxyl radicals promotes the photocatalytic disinfection, which is consistent with the results of other researchers [16].

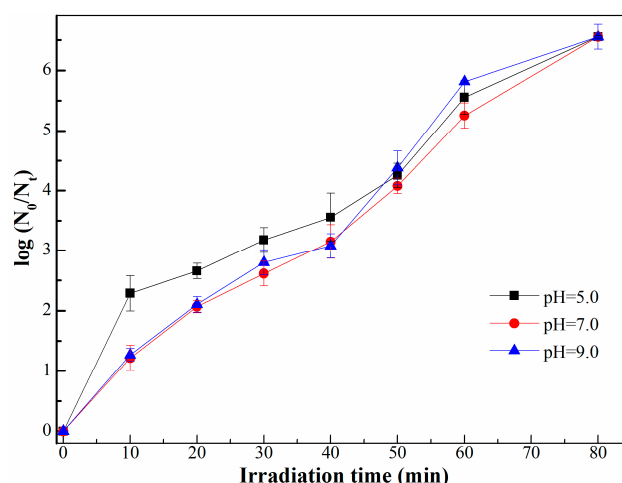


Figure 7. Effect of pH on the photocatalytic removal efficiency of bacteriophage f2.

2.2.3. Effect of Humic Acid

Humic acid is one of the major natural organic matters and widely exists in natural water. According to the concentration range of humic acid in the actual water body, the effects of humic acid

with different concentrations (0, 0.5, 1.0, and 1.5 mg·L⁻¹) on photocatalytic disinfection by AgCN composite photocatalysts were investigated and the results are shown in Figure 8.

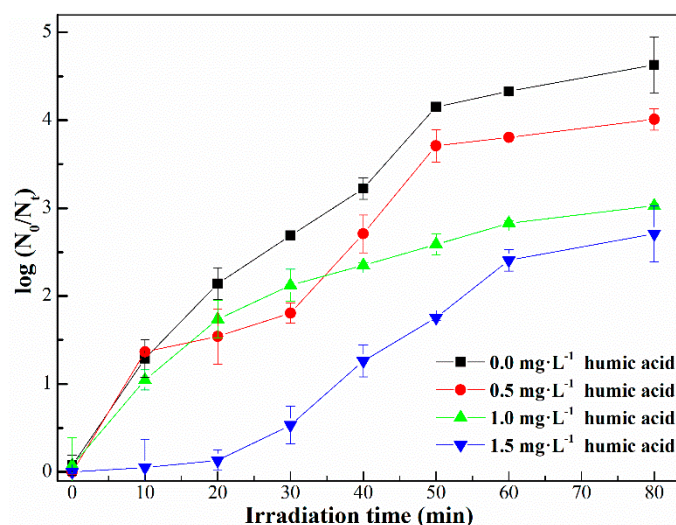


Figure 8. Effect of humic acid on the photocatalytic inactivation towards the bacteriophage f2.

It is obvious that, with the increase of concentration of humic acid, the removal efficiency of bacteriophage f2 by AgCN photocatalysts is decreased. The removal efficiency of f2 is 4.01 log, 2.96 log, and 2.63 log, respectively, when the concentration of humic acid is 0.5, 1.0, and 1.5 mg·L⁻¹. Concentrations of humic acid above 1.0 mg·L⁻¹ have a huge impact. The possible reason is that a broad spectrum of light from 270 to 500 nm could be absorbed by humic acid, which could further protect the photocatalysts against irradiation of visible light [28].

2.2.4. Reusability of AgCN Composite Photocatalysts

In the practical application of novel photocatalysts, the reusability of the material itself is one of the key indicators. Thus, to further verify the stability, reusability and reutilization of AgCN composite, additional experiments were carried out under the irradiation of visible light. The AgCN composite was naturally sedimented for 30 min, and then the sediments at the bottom of the reactor were collected for the next cycle. The results of cycling inactivation experiments are displayed in Figure 9.

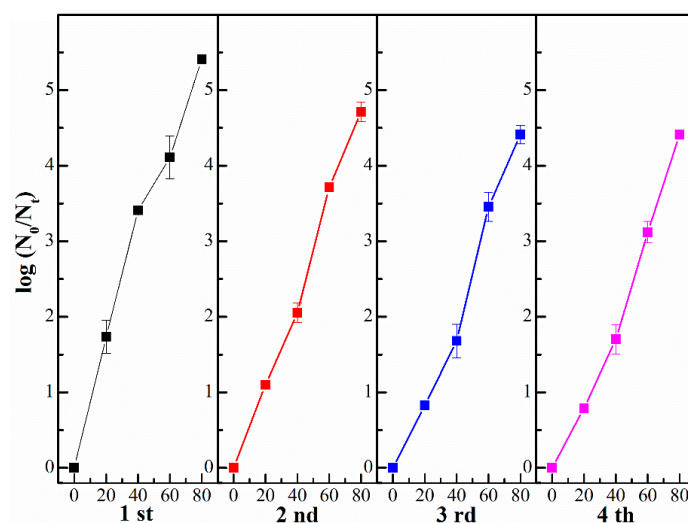


Figure 9. Cycling experiments of bacteriophage f2 by AgCN composite photocatalysts under visible light irradiation.

In Figure 9, it could be seen that, with the increase of reuse times, although the inactivation rate of bacteriophage f2 in water decreased to a certain extent, it remained around 4 log, which indicates excellent inactivation performance. In addition, during the experiments, it can be found that the AgCN composite after reaction still has good color and shape (faint yellow) compared with the single Ag_3PO_4 particles after reaction (brownish black). This means that the problem of easy oxidation of Ag_3PO_4 catalysts is effectively alleviated by combined AgCN composite, which is consistent with the literature [14,18,20]. Therefore, the AgCN photocatalysts have excellent stability of photocatalytic activity, which demonstrates that AgCN composite is stable visible-light photocatalyst and could be reused in inactivation of microbial contaminated water.

2.3. Inactivation Mechanisms of Bacteriophage f2

Active radical trapping experiments were designed to investigate thoroughly the main free radicals of photocatalytic inactivation. Photogenerated holes (h^+), photogenerated electrons (e^-), hydroxyl radicals ($\cdot\text{OH}$), and superoxide ion radicals ($\cdot\text{O}_2^-$) are often regarded as the reactive species in photocatalytic process. Therefore, in the experimental design, h^+ , e^- , $\cdot\text{O}_2^-$ and $\cdot\text{OH}$ were trapped by 5 mM of sodium oxalate, potassium dichromate, 4-hydroxy-2,2,6,6-tetramethylpiperidin-1-oxyl (TEMPO), and isopropanol, respectively. The experimental results are shown in Figure 10.

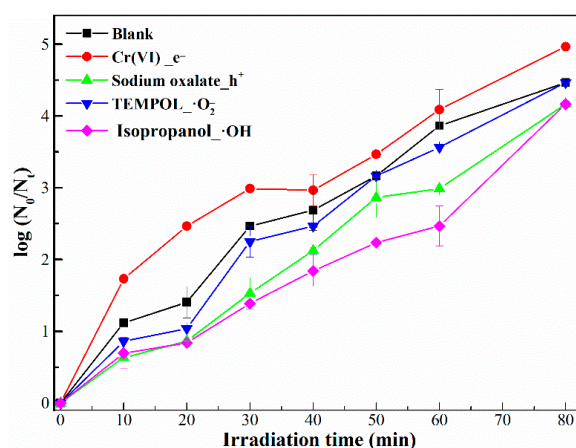


Figure 10. Effect of different active radical scavengers on photocatalytic inactivation of bacteriophage f2 by AgCN composite photocatalysts.

In Figure 10, it can be seen that the removal efficiency decreased with the adding of h^+ scavengers, while the efficiency increased to some extent with the addition of e^- scavengers, indicating that h^+ plays a major role in the first step of the photocatalytic reaction ($\text{AgCN} + h\nu \rightarrow e^- + h^+$). Meanwhile, $\cdot\text{O}_2^-$ radicals do not play a primary role in photocatalytic inactivation of bacteriophage f2. With the addition of $\cdot\text{OH}$ radicals' scavengers, the photocatalytic inactivation efficiency is greatly decreased, indicating that $\cdot\text{OH}$ radicals play a more important role in the whole system. As stated above, h^+ radicals are the main active species contributing to the virus inactivation by AgCN composite [16].

According to the above discussion, a possible photocatalytic inactivation mechanism of the AgCN composite photocatalysts is proposed, as shown in Figure 11. When $g\text{-C}_3\text{N}_4$ and Ag_3PO_4 are effectively combined, the valence band (VB) potentials and the conduction band (CB) potentials of the photocatalysts can be theoretically calculated with Equations (2) and (3) [29]:

$$E_{CB} = X - E_C - 0.5E_g \quad (2)$$

$$E_{VB} = E_{CB} + E_g \quad (3)$$

where X is the absolute electronegativity of a semiconductor; E_C is the energy of free electrons vs. hydrogen (≈ 4.5 eV); and E_g represents the band-gap of the photocatalysts.

According to Figure 6b, the E_g values of $g\text{-C}_3\text{N}_4$ and Ag_3PO_4 are calculated as 2.49 and 2.13 eV, respectively. Meanwhile, the X values for the as-prepared Ag_3PO_4 and $g\text{-C}_3\text{N}_4$ are 5.93 and 4.72 eV, respectively. Then, according to the Mulliken electronegativity theory (Equations (2) and (3)), the conduction band (CB) and valence band (VB) of $g\text{-C}_3\text{N}_4$ are calculated as -1.00 eV and $+1.49$ eV, respectively. The CB and VB of Ag_3PO_4 are calculated as $+0.37$ eV and $+2.50$ eV, respectively. According to the theory of typical heterojunction [17], photogenerated holes (h^+) from the VB of Ag_3PO_4 can be transferred into the corresponding VB of $g\text{-C}_3\text{N}_4$. Meanwhile, photoexcited electrons (e^-) from the VB of $g\text{-C}_3\text{N}_4$ can be transferred into the corresponding CB of Ag_3PO_4 . However, the h^+ in the VB of $g\text{-C}_3\text{N}_4$ cannot effectively generate hydroxyl radicals ($\cdot\text{OH}$), which is contrary to the experimental results of free radical scavengers. To better explain the enhanced photocatalytic performance of AgCN composite, Z-scheme photocatalytic mechanism was given, as shown in Figure 11.

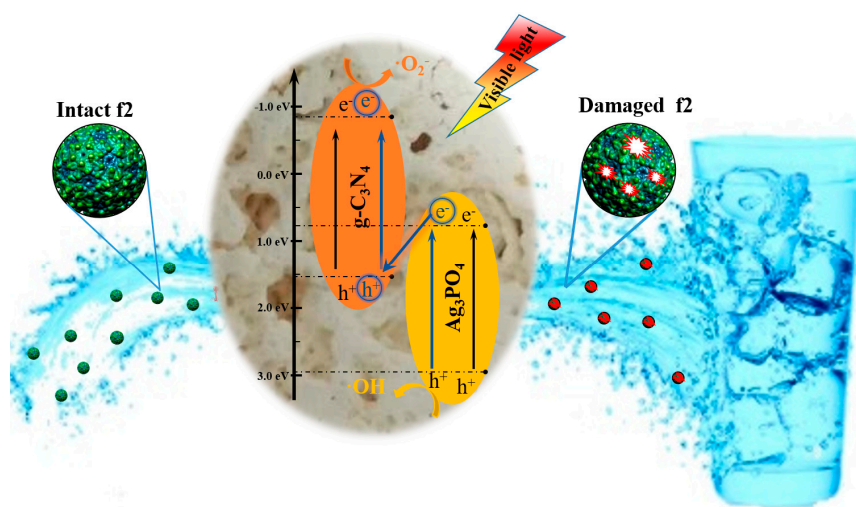


Figure 11. The possible mechanism of photocatalytic inactivation of bacteriophage f2 by the AgCN photocatalysts under visible light irradiation.

Both $g\text{-C}_3\text{N}_4$ and Ag_3PO_4 can be irradiated to generate electron–hole pairs under visible light irradiation, and the photoexcited electrons from the VB of $g\text{-C}_3\text{N}_4$ and Ag_3PO_4 can be easily transferred into the corresponding CB of $g\text{-C}_3\text{N}_4$ and Ag_3PO_4 . Meanwhile, photoinduced electrons from the conduction band (CB) of Ag_3PO_4 would be easily transferred to the valence band (VB) of $g\text{-C}_3\text{N}_4$. Then, the electrons stored in CB of $g\text{-C}_3\text{N}_4$ are trapped by dissolved oxygen near the surface of $g\text{-C}_3\text{N}_4$ in water to form reactive superoxide radical ion ($\cdot\text{O}_2^-$). In addition, the holes (h^+) in the VB of Ag_3PO_4 could react with H_2O or OH^- near the surface of Ag_3PO_4 to form hydroxyl radicals ($\cdot\text{OH}$). Then, the bacteriophage f2 are oxidized by these highly active $\cdot\text{OH}$ radical species, photogenerated holes (h^+), and superoxide radical ($\cdot\text{O}_2^-$). As a result, the photogenerated electron–hole pairs of Ag_3PO_4 and $g\text{-C}_3\text{N}_4$ photocatalysts are spatially separated, which improves the corresponding photocatalytic oxidation ability.

3. Materials and Methods

3.1. Materials and Chemicals

All chemicals used in this study were of analytical grade and not further purified. Sodium dihydrogen phosphate (NaH_2PO_4), urea ($\text{CO}(\text{NH}_2)_2$), and silver nitrate (AgNO_3) were purchased from Xilong Scientific Co., Ltd. (Guangdong, China). All solutions were prepared with ultra-pure water from an arium[®] pro VF | UF system (Sartorius, Germany). In addition, bacteriophage f2 and its host bacteria (*E. coli* 285) were purchased from institute of Hygiene and Environmental Medicine (Academy of Military Medical Sciences, Beijing, China). The duplication and purification process of bacteriophage f2 followed the method described in a previous research [27].

3.2. Preparation of $g\text{-C}_3\text{N}_4$

In general, $g\text{-C}_3\text{N}_4$ photocatalysts were prepared by the thermal polymerization method using urea as a precursor. In a typical process, 10 g urea powder and 15 mL ultrapure water was mixed in a beaker and then dried in an oven at 60 °C for 10 h. After cooling down to room temperature naturally, the bulk urea was collected and ground into fine powders. Then, the fine powders were placed in a muffle furnace and heated to 550 °C at 5 °C/min and subsequently maintained at 550 °C for 3 h. After cooling down to room temperature naturally, the gained products were collected, and washed three times with ethanol and pure water, respectively, put in an oven for 10 h at 60 °C, and then ground into fine powders again.

3.3. Preparation of the $\text{Ag}_3\text{PO}_4/g\text{-C}_3\text{N}_4$ Composite

In this study, the $\text{Ag}_3\text{PO}_4/g\text{-C}_3\text{N}_4$ (AgCN) composite was synthesized via in-situ solvothermal method, as shown in Figure 12. In brief, 1.0 g of $g\text{-C}_3\text{N}_4$ powders, prepared by the means described in Section 3.2, was uniformly dispersed in the ultra-pure water of 50 mL by ultrasound with 0.3 kW. Then, 0.5 mmol of silver nitrate (AgNO_3) was dissolved in 10 mL ultra-pure water to form a homogeneous solution and then dropped into the solution of $g\text{-C}_3\text{N}_4$ by stirring for 1 h. Then, the 10 mL 0.5 mol/L sodium dihydrogen phosphate (NaH_2PO_4) solution was injected into the above solutions at the speed of 5 mL/min by constant-flow pump and continuously stirred for 1 h at ambient temperature. Then, the homogeneous solution was poured into a Teflon[®] autoclave (Zhonghuan Lab Furnace Co., Ltd., Tianjin, China) with a total volume of 50 cm³, followed by the hydrothermal reaction at 150 °C for 10 h. The pale-yellow powder products were separated by filter pump with 0.22 μm filter membrane, washed alternately with ultra-pure water and ethanol three times, respectively, and then dried in a draught drying cabinet at 60 °C for another 10 h. The products were denoted as AgCN composite. In addition, the single Ag_3PO_4 photocatalysts were synthesized based on the above method without adding the $g\text{-C}_3\text{N}_4$.

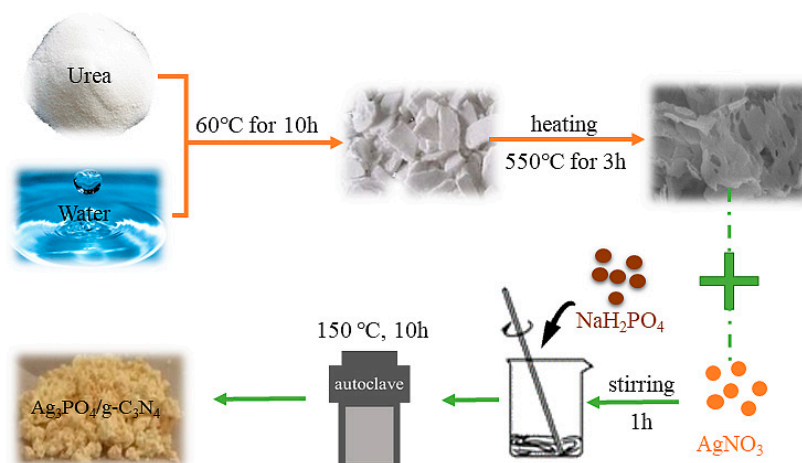


Figure 12. Schematic route for the synthesis of AgCN photocatalysts.

3.4. Characterization

The main crystalline phase of the prepared photocatalysts was determined by X-ray diffraction analysis. The size and morphology of synthesized materials was observed by scanning electron microscope (SEM, Hitachi S-4800, Hitachi, Ltd., Tokyo, Japan). A UV-vis diffusive reflective spectrophotometer (DRS, Agilent, Cary 6000i, Agilent Technologies Inc., Santa Clara, CA, USA) was employed to measure the capacity of UV-vis absorption and estimate the bandgap of the photocatalysts, employing BaSO_4 powders as a reference. Photoluminescence spectra (PLS) were recorded on a fluorescence spectrophotometer F-7000 (Hitachi, Ltd., Tokyo, Japan) at ambient temperature. The N_2 adsorption–desorption isotherms were measured by an Autosorb-IQ Automated Gas Sorption

Analyzer (Quantachrome Instruments, Boynton Beach, FL, USA) at 80 °C. The specific surface area was calculated by the Brunauer–Emmett–Teller (BET) method.

3.5. Photocatalytic Disinfection Experiment

3.5.1. Experimental Installation

The photocatalytic disinfection experiments were carried out in a multisite photocatalytic reactor, as shown in Figure 13. The transparent reaction tube was a 100 mL glass tubes with certain optical properties. The cooling water system with a double-walled cooling-water hollow tube and Xenon lamp source were turned on sequentially, and the experiments were carried out until the light intensity and temperature of reaction stabilized. The source of visible light was provided by a CEL-HXUV300 Xenon lamp (Beijing ZhongJiaoJinYuan Tech Co. Ltd., Beijing, China) with a 400 nm cut-off filter, and the visible light intensity was adjusted to 30 mW·cm⁻². The pH values of all solutions were adjusted with 0.1 M hydrochloric acid (HCl) and sodium hydroxide (NaOH) solution. To make the solution uniform, the reactive solutions were dispersed by magnetic stirring during the experiment. Moreover, the experimental results were obtained through three parallel experiments, and the corresponding error lines are accurately marked in figures.

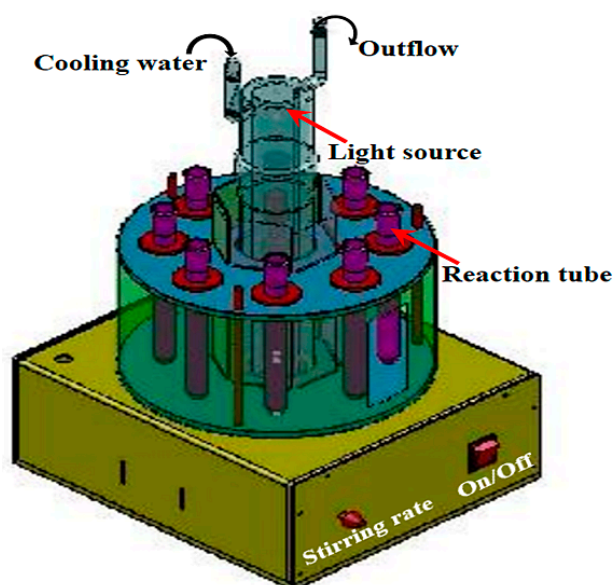


Figure 13. Diagrammatic sketch of the photocatalytic disinfection reactor system.

3.5.2. Culture and Counting of Bacteriophage f2

In this study, all glass and plastic implements used in the experiments were autoclaved for 30 min at 121 °C by the high-pressure steam sterilization pot. The bacteriophage f2 were cultured at 37 °C and 150 rpm for 15 h in a shaking incubator. The final cell density was adjusted to about 10⁶ PFU/mL, using ultrapure water for the further disinfection experiment.

Generally, 80 mL of bacteriophage f2 solution and 5 mg of photocatalysts were mixed with a magnetic stirrer under visible light. During the disinfection process, the mixture was withdrawn by pipette at planned time intervals, and the concentrations of virus were calculated using the double agar plate method [30]. The disposable petri dishes were placed in a biochemical incubator at 37 °C for 4 h, and the number of bacteriophage plaque was enumerated by visual inspection. When counting, the number of transparent plaques of 30–300 was regard as the valid value and used for further analysis. The inactivation effect of bacteriophage f2 was calculated with Equation (4):

$$Re = \log_{10}N_0 - \log_{10}N_t = \log_{10}(N_0/N_t) \quad (4)$$

where Re represents the removal efficiency of virus, t is the irradiation time, and N_0 and N_t are the concentrations of virus at the initial time and time t , respectively.

4. Conclusions

A highly-efficient, stable, and visible-light-driven photocatalyst, AgCN, was prepared by a facile and reproducible in situ precipitation method and applied in viral inactivation in water. The bandgap of the material is 2.34 eV, which has a wider light response compared to that of traditional photocatalysts (TiO₂ and ZnO). By effective combination of two semiconductors (Ag₃PO₄, and g-C₃N₄), a stronger visible light response and lower carrier recombination rate can be achieved compared with single photocatalyst. The photocatalytic inactivation efficiency of bacteriophage f2 by AgCN composite photocatalysts reached 6.5 log within 80 min under visible light irradiation, which is attributed mainly to the synergistic effect of g-C₃N₄ and Ag₃PO₄, e.g., the excellent separation of the photogenerated electrons and holes, and wider visible light response. The order of the radicals during the photocatalytic inactivation of bacteriophage f2 is: $\cdot\text{OH} > \text{h}^+ > \cdot\text{O}_2^-$. This study successfully provides a kind of promising photocatalyst to viral inactivation in pathogenic microorganism polluted water.

Author Contributions: R.C. and L.S. contributed to the writing of this paper. J.Y. and S.X. contributed to the experiment operation of this paper. R.C. and X.Z. contributed to the conception and revision of this paper.

Funding: This work was supported by the National Natural Science Foundation of China (Grant Nos. 51778618 and 51478460), which is greatly acknowledged.

Acknowledgments: L.S. especially wants to thank the care and spiritual support from Jin-lei Wei over the past decade. I know what love is because of you.

Conflicts of Interest: The authors declare no conflict of interest.

References

1. Prevost, B.; Goulet, M.; Lucas, F.S.; Joyeux, M.; Moulin, L.; Wurtzer, S. Viral persistence in surface and drinking water: Suitability of pcr pre-treatment with intercalating dyes. *Water Res.* **2016**, *91*, 68–76. [[CrossRef](#)] [[PubMed](#)]
2. Gibson, K.E. Viral pathogens in water: Occurrence, public health impact, and available control strategies. *Curr. Opin Virol.* **2014**, *4*, 50–57. [[CrossRef](#)] [[PubMed](#)]
3. Gall, A.M.; Mariñas, B.J.; Lu, Y.; Shisler, J.L. Waterborne viruses: A barrier to safe drinking water. *PLoS Pathog.* **2015**, *11*, e1004867. [[CrossRef](#)] [[PubMed](#)]
4. Zhang, Q.; Liu, B.; Liu, Y.; Cai, X.; Liu, X.; Dai, R. Removal and inactivation of virus by drinking water treatment in the presence of bromide or iodide. *J. Water Chem. Technol.* **2015**, *37*, 96–101. [[CrossRef](#)]
5. Zyara, A.; Torvinen, E.; Veijalainen, A.-M.; Heinonen-Tanski, H. The effect of uv and combined chlorine/uv treatment on coliphages in drinking water disinfection. *Water* **2016**, *8*, 130. [[CrossRef](#)]
6. Rodriguez, R.A.; Bounty, S.; Beck, S.; Chan, C.; McGuire, C.; Linden, K.G. Photoreactivation of bacteriophages after uv disinfection: Role of genome structure and impacts of uv source. *Water Res.* **2014**, *55*, 143–149. [[CrossRef](#)] [[PubMed](#)]
7. Liga, M.V.; Bryant, E.L.; Colvin, V.L.; Li, Q. Virus inactivation by silver doped titanium dioxide nanoparticles for drinking water treatment. *Water Res.* **2011**, *45*, 535–544. [[CrossRef](#)] [[PubMed](#)]
8. Liu, J.; Liu, Y.; Liu, N.; Han, Y.; Zhang, X.; Huang, H.; Lifshitz, Y.; Lee, S.-T.; Zhong, J.; Kang, Z. Metal-free efficient photocatalyst for stable visible water splitting via a two-electron pathway. *Science* **2015**, *347*, 970–974. [[CrossRef](#)] [[PubMed](#)]
9. Martha, S.; Nashim, A.; Parida, K.M. Facile synthesis of highly active g-C₃N₄ for efficient hydrogen production under visible light. *J. Mater. Chem. A* **2013**, *1*, 7816–7824. [[CrossRef](#)]
10. Sun, S.; Liang, S. Recent advances in functional mesoporous graphitic carbon nitride (mpg-C₃N₄) polymers. *Nanoscale* **2017**, *9*, 1544–1578. [[CrossRef](#)] [[PubMed](#)]
11. Wang, Y.; Wang, X.; Antonietti, M. Polymeric graphitic carbon nitride as a heterogeneous organocatalyst: From photochemistry to multipurpose catalysis to sustainable chemistry. *Angew. Chem. Int. Ed.* **2011**, *51*, 68–89. [[CrossRef](#)] [[PubMed](#)]

12. Yu, H.; Shi, R.; Zhao, Y.; Bian, T.; Zhao, Y.; Zhou, C.; Waterhouse, G.I.N.; Wu, L.-Z.; Tung, C.-H.; Zhang, T. Alkali-assisted synthesis of nitrogen deficient graphitic carbon nitride with tunable band structures for efficient visible-light-driven hydrogen evolution. *Adv. Mater.* **2017**, 1605148. [[CrossRef](#)] [[PubMed](#)]
13. Gao, D.; Xu, Q.; Zhang, J.; Yang, Z.; Si, M.; Yan, Z.; Xue, D. Defect-related ferromagnetism in ultrathin metal-free g-C₃N₄ nanosheets. *Nanoscale* **2014**, 6, 2577. [[CrossRef](#)] [[PubMed](#)]
14. Ma, S.; Zhan, S.; Jia, Y.; Shi, Q.; Zhou, Q. Enhanced disinfection application of ag-modified g-C₃N₄ composite under visible light. *Appl. Catal. B Environ.* **2016**, 186, 77–87. [[CrossRef](#)]
15. Hong, J.; Xia, X.; Wang, Y.; Xu, R. Mesoporous carbon nitride with in situ sulfur doping for enhanced photocatalytic hydrogen evolution from water under visible light. *J. Mater. Chem.* **2012**, 22, 15006. [[CrossRef](#)]
16. Deng, J.; Liang, J.; Li, M.; Tong, M. Enhanced visible-light-driven photocatalytic bacteria disinfection by g-C₃N₄-AgBr. *Colloid Surf. B* **2017**, 152, 49–57. [[CrossRef](#)]
17. Hong, Y.; Jiang, Y.; Li, C.; Fan, W.; Yan, X.; Yan, M.; Shi, W. In-situ synthesis of direct solid-state z-scheme V₂O₅/g-C₃N₄ heterojunctions with enhanced visible light efficiency in photocatalytic degradation of pollutants. *Appl. Catal. B Environ.* **2016**, 180, 663–673. [[CrossRef](#)]
18. Sulaeman, U.; Febiyanto, F.; Yin, S.; Sato, T. The highly active saddle-like Ag₃PO₄ photocatalyst under visible light irradiation. *Catal. Commun.* **2016**, 85, 22–25. [[CrossRef](#)]
19. Yeo, B.-E.; Seo, Y.; Park, H.; Huh, Y.-D. Facet effect of Ag₃PO₄ crystals on antibacterial activities. *Bull. Korean Chem. Soc.* **2015**, 36, 1904–1907. [[CrossRef](#)]
20. Kumar, S.; Surendar, T.; Baruah, A.; Shanker, V. Synthesis of a novel and stable g-C₃N₄-Ag₃PO₄ hybrid nanocomposite photocatalyst and study of the photocatalytic activity under visible light irradiation. *J. Mater. Chem. Coruña* **2013**, 1, 5333. [[CrossRef](#)]
21. Thomas, A.; Fischer, A.; Goettmann, F.; Antonietti, M.; Müller, J.-O.; Schlögl, R.; Carlsson, J.M. Graphitic carbon nitride materials: Variation of structure and morphology and their use as metal-free catalysts. *J. Mater. Chem.* **2008**, 18, 4893. [[CrossRef](#)]
22. Sun, J.-X.; Yuan, Y.-P.; Qiu, L.-G.; Jiang, X.; Xie, A.-J.; Shen, Y.-H.; Zhu, J.-F. Fabrication of composite photocatalyst g-C₃N₄-ZnO and enhancement of photocatalytic activity under visible light. *Dalton Trans.* **2012**, 41, 6756. [[CrossRef](#)] [[PubMed](#)]
23. Zhang, Y.; Liu, J.; Wu, G.; Chen, W. Porous graphitic carbon nitride synthesized via direct polymerization of urea for efficient sunlight-driven photocatalytic hydrogen production. *Nanoscale* **2012**, 4, 5300. [[CrossRef](#)] [[PubMed](#)]
24. Wang, F.; Chen, P.; Feng, Y.; Xie, Z.; Liu, Y.; Su, Y.; Zhang, Q.; Wang, Y.; Yao, K.; Lv, W.; et al. Facile synthesis of n-doped carbon dots/g-c 3 n 4 photocatalyst with enhanced visible-light photocatalytic activity for the degradation of indomethacin. *Appl. Catal. B Environ.* **2017**, 207, 103–113. [[CrossRef](#)]
25. Zhang, C.; Li, Y.; Zhang, W.; Wang, P.; Wang, C. Metal-free Virucidal effects induced by g-C₃N₄ under visible light irradiation: Statistical analysis and parameter optimization. *Chemosphere* **2018**, 195, 551–558. [[CrossRef](#)] [[PubMed](#)]
26. O'Regan, B.; Grätzel, M. A low-cost, high-efficiency solar cell based on dye-sensitized colloidal TiO₂ films. *Nature* **1991**, 353, 737–740. [[CrossRef](#)]
27. Zhang, X.; Zhang, L.; Xie, T.; Wang, D. Low-temperature synthesis and high visible-light-induced photocatalytic activity of bio/tio₂heterostructures. *J. Phys. Chem. C* **2009**, 113, 7371–7378. [[CrossRef](#)]
28. Zheng, X.; Shen, Z.; Cheng, C.; Shi, L.; Cheng, R.; Dong, J. Electrospinning Cu-TiO₂ nanofibers used for photocatalytic disinfection of bacteriophage f2: Preparation, optimization and characterization. *RSC Adv.* **2017**, 7, 52172–52179. [[CrossRef](#)]
29. Muela, A.; Garcia-Bringas, J.M.; Arana, I.; Barcina, I. Humic Materials Offer Photoprotective Effect to *Escherichia coli* Exposed to Damaging Luminous Radiation. *Microb. Ecol.* **2000**, 40, 336–344. [[CrossRef](#)] [[PubMed](#)]
30. Cheng, R.; Li, G.; Shi, L.; Xue, X.; Kang, M.; Zheng, X. The mechanism for bacteriophage f2 removal by nanoscale zero-valent iron. *Water Res.* **2016**, 105, 429–435. [[CrossRef](#)] [[PubMed](#)]

